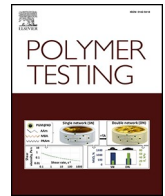


A cost-effective protocol for detecting fluorescent microplastics in arable soils to study redistribution processes

Saunak Sinha Ray, David Zumr, Florian Wilken, Tomáš Dostál, Peter Fiener

Angaben zur Veröffentlichung / Publication details:

Sinha Ray, Saunak, David Zumr, Florian Wilken, Tomáš Dostál, and Peter Fiener. 2025. "A cost-effective protocol for detecting fluorescent microplastics in arable soils to study redistribution processes." *Polymer Testing* 147: 108824.
<https://doi.org/10.1016/j.polymertesting.2025.108824>.



A cost-effective protocol for detecting fluorescent microplastics in arable soils to study redistribution processes

Saunak Sinha Ray^{a,*}, David Zumr^{a,**}, Florian Wilken^b, Tomáš Dostál^a, Peter Fiener^b

^a Department of Landscape Water Conservation, Faculty of Civil Engineering, Czech Technical University in Prague, 16629, Prague, Czech Republic

^b University of Augsburg, Institute of Geography, Alter Postweg 118, 86159, Augsburg, Germany

ARTICLE INFO

Keywords:

Soil
Sediment monitoring
Surface runoff
Microplastic transport
Identification
Fluorescence

ABSTRACT

Understanding microplastics' (MPs) transport from soils to aquatic ecosystems is challenging due to labor-intensive detection methods, especially in large-scale plot experiments analyzing surface runoff and soil erosion. To address this, we used fluorescent MPs as tracers and developed a cost-effective protocol to detect them in dry soils and eroded sediments. We analyzed spherical polyethylene (PE: 125–150 μm ; 425–500 μm) and irregular polylactic acid (PLA: 125–150 μm ; 250–300 μm). Sample assays were prepared primarily based on dry and wet sieving. Subsequent darkroom photography under 365 nm illumination, and thresholding and segmentation-based image analysis were done. The developed protocol demonstrates high reliability, precision, and F-scores of $88.7\% \pm 2.9\%$, $85.2\% \pm 3.1\%$, and $86.9\% \pm 2.8\%$. PE exhibited slightly higher recovery rates ($85\% \pm 5\%$) than PLA ($79\% \pm 8\%$). Particle size influenced recovery, with larger MPs achieving significantly higher recovery. Smaller particles showed slightly lower recovery under dry soil conditions, but their recovery improved under sediment conditions facilitated by wet sieving and ultrasonication. All fluorescent MPs retained $>95\%$ detectability after three months of storage, highlighting marker temporal stability. Compared to existing methods, this protocol eliminates complex digestion steps, reduces costs, and ensures minimal contamination, providing a robust framework for MP transport studies. It offers potential for enhancement through advanced imaging and machine learning, enabling more efficient and accessible detection in environmental research.

1. Introduction

Microplastics (MPs), mainly defined as plastic fragments between 1 μm and 5 mm, have become a pressing environmental issue due to their pervasive presence in water [1], sediments [2], soils [3], and air [4]. Increasing evidence indicates that microplastic pollution in agricultural soils may far exceed that in oceans [5]. This pollution is especially alarming in agroecosystems, which are critical for food production. Modern agriculture increasingly relies on plastic products, including mulching films [6], greenhouse coverings [7], wraps, coatings [8], piping systems [9], and silage labels [10]. While these materials offer cost-effective durability, their widespread use contributes significantly to soil MP accumulation. Additional sources, such as compost [11] and sewage sludge [12] as fertilizers, irrigation water [13], and indirect transport mechanisms like wind [14], water [15], and tire wear [16] exacerbate the issue. Once introduced into soils, macro- and

microplastics undergo fragmentation, further amplifying contamination.

This poses a global threat to terrestrial environments and agroecosystems [17,18]. Recent investigations reveal a substantial presence of MPs in agricultural topsoil [19,20], with farming practices and soil heterogeneity facilitating lateral transport via surface runoff and soil erosion, potentially transporting these particles to aquatic systems [21]. Vertical infiltration, driven by rainfall or irrigation, facilitates the downward migration of MPs through soil macropores [22], raising concerns about groundwater entry [23].

The movement of MPs in terrestrial environments remains poorly understood, underscoring the pressing need for research into their fate and transport to evaluate the impacts of soil microplastic pollution [24, 25]. Recent studies have investigated horizontal transport mechanisms, such as erosion, through field experiments [26,27] and laboratory setups [17,28], as well as modeling-based analysis [29]. Vertical transport studies have primarily used column experiments to examine infiltration

This article is part of a special issue entitled: Nano/Microplastic Testing published in Polymer Testing.

* Corresponding author.

** Corresponding author.

E-mail addresses: saunak.sinha.ray@fsv.cvut.cz (S. Sinha Ray), David.Zumr@fsv.cvut.cz (D. Zumr).

<https://doi.org/10.1016/j.polymeresting.2025.108824>

Received 23 December 2024; Received in revised form 7 April 2025; Accepted 24 April 2025

Available online 26 April 2025

0142-9418/© 2025 The Authors. Published by Elsevier Ltd. This is an open access article under the CC BY license (<http://creativecommons.org/licenses/by/4.0/>).

Abbreviations

| | |
|-------|-----------------------|
| MP = | Microplastic |
| PLA = | Polylactic Acid |
| PE = | Polyethylene |
| UV = | Ultraviolet radiation |

processes [30,31]. These experiments typically introduce MPs of varying polymer types, shapes, and sizes into the soil system and simulate rainfall to analyze MP fate and transport behaviors. For easier identification, researchers often use microplastic particles with bright or non-native colors (e.g. white, pink) [26,32]. Recovery of these induced MPs from soil and sediment samples is commonly achieved through density separation and different procedures to destroy organic matter components [33,34]. Visual identification may be useful with larger MP sizes, making it cost-effective and straightforward [43], but it is prone to bias, misidentification and is difficult to standardize [55]. More robust identification methods include stereomicroscopy and Fourier transform infrared spectroscopy (FTIR) [35], which are more reliable but require significant time, sample preparation, and access to costly instrumentation [44,45].

Fluorescence-based methods have gained traction in MP analysis as an alternative to conventional visual or spectroscopic detection. One widely applied approach is Nile Red staining [56], a lipophilic dye that binds to hydrophobic plastic surfaces and fluoresces under UV or blue light. It has shown utility across various polymer types and is compatible with automated imaging and software-based image analysis, improving throughput [36,40–42]. However, Nile Red staining has its limitations. It is prone to non-specific staining of natural organic matter, exhibits inconsistent fluorescence among polymer types, and is particularly susceptible to background interference in complex soil matrices [46]. These drawbacks hinder reliable detection, especially at low MP concentrations. Furthermore, automated analysis pipelines inherit these challenges, often requiring extensive image pre-processing, manual threshold tuning, and calibration to separate MPs from background artifacts [47]. UV-labeled microplastics and direct imaging approaches have been increasingly explored to address these limitations. These methods bypass staining altogether by incorporating fluorescent markers directly into the polymer matrix. In sediment transport studies, such fluorescent tagging—using tracers like rhodamine or anthracene-coated particles—has been instrumental in tracking particle movement with high precision [37,38]. Despite their promise, these tracers are not routinely applied in MP research due to high costs, dye degradation, and limited suitability for soils with strong background fluorescence or organic content [23,39].

Unlike studies focusing on native environmental microplastic pollution, experimental designs in microplastic transport research offer the advantage of pre-selecting MP polymer shape, size, and color. This controlled approach enables researchers to optimize precise MP extraction and identification recovery techniques. Despite substantial progress in MP transport research and the development of various protocols, there remains a critical need for detection methods that are fast, cost-effective, accurate, and reliable. Building on existing advancements, this study introduces a simplified protocol using pre-labeled fluorescent MPs and darkroom UV imaging, tailored for tracer-based MP redistribution experiments. Such advancements are pivotal for minimizing the costs and time associated with laboratory analyses while enabling the study of MP transport processes across larger sample sets. This is particularly important for capturing diverse environmental conditions and temporal dynamics, with a special focus on sediment transport phenomena.

To address this gap, we conducted laboratory experiments to analyze fluorescent microplastics in two treatment scenarios: (1) dry soil and (2)

wet soil or runoff-eroded sediment to mirror a simulated runoff scenario. Two UV-labeled fluorescent polymers were tested: (1) spherical polyethylene (PE) microspheres, sourced as commercially available microplastic particles, and (2) polylactic acid (PLA) filament, an economical and accessible material grounded into irregularly shaped microplastic particles/fragments. Using a simple darkroom photography setup and UV light, we aimed to answer the following research questions:

1. Can fluorescent PE and PLA MP particles in the 125–500 μm range be identified directly from soil and sediment without requiring extraction?
2. How do recovery rates vary depending on MP size and shape?
3. Is the protocol sensitive to particle concentration, ranging from low to high MP particle counts?
4. Are there differences in the applicability of the two UV-labeled fluorescent MP polymer types as proxy tracers in microplastic transport studies?

2. Materials and methods

2.1. Microplastic (MP)

The protocol development focused on the MP size distribution of 125–500 μm , aligning with sizes used in previous MP transport studies [26–28,48], to ensure comparability of results. This size range is well-established in MP transport literature and aligns with experimental requirements for tracer visibility and non-destructive imaging under UV fluorescence.

Uniform fluorescent PE microspheres were sourced from Cospheric LLC (Santa Barbara, USA) in two distinct colors and size ranges: green (125–150 μm) and red (425–500 μm). These microspheres have 1–1.09 g cm^{-3} densities and a melting point of 110–130 $^{\circ}\text{C}$. The manufacturer reported that the fluorophore is homogeneously incorporated into the PE matrix, making it solvent-resistant.

Irregular UV-fluorescence-labeled PLA MP particles were produced from a commercially available 1.75 mm fluorescent PLA filament (Filament-PM, Prague, Czech Republic), selected for its biodegradable properties, low cost, widespread availability, and compatibility with cryo-milling procedures [49]. The filaments were cryogenically frozen with liquid nitrogen, mechanically milled into irregularly shaped fragments, and industrially sieved by Lavaris Ltd. Czech Republic (<http://www.lavaris.eu/>). Additional dry sieving was conducted in the laboratory to achieve precise size fractions. Two fluorescent PLA particle size ranges were used: orange (125–150 μm) and green (250–300 μm). These particles have a 1.24 g cm^{-3} density and a melting point of 150–160 $^{\circ}\text{C}$. Stereomicroscope imaging (Zeiss Axio Zoom.V16) was performed on 200 particles from each PE and PLA size fraction to verify the size distributions. The uniform distribution of particle sizes was confirmed using QQ plots.

2.2. Soil

Loamy soil, classified as Cambisol, was selected due to its prevalence as Central Europe's most common agricultural soil type [50]. The soil, characterized by 18.3 % clay, 33.8 % silt, 47.9 % sand, 4.1 % organic matter, and a pH (KCl) of 7.12, was sourced from an agricultural field in Řisuty, Czech Republic (50°13'2.0"N, 14°1'2.2"E). Topsoil was collected from 0 to 15 cm depth across fifteen locations within the field using a metal spade and thoroughly mixed to ensure homogeneity. Plant roots and stones were manually removed during the process. The soil was then air-dried and sieved through a 2 mm mesh to produce a uniform sample for experimental use.

2.3. Darkroom photography setup

The photography analysis was conducted in a pop-up dark tent

(Ilford Pop Up Darkroom) measuring 1.3 m × 1.3 m × 2.2 m, illuminated by fluorescent lights. A modified table stand was built to place and photograph the MP assays. The table had two vertical stands with a platform area on which the MP assays were placed. The camera (Sony Alpha model α6000 with a Sony SEL16F28 lens) was placed on the bottom stand at a 90° angle directly above the filter. The height of this stand was adjustable, allowing manual camera focusing. The UV lamp (Iradifire, 48 × 1W array, 365 nm, UV Gear, UK) was installed on the stand above at a 45° angle for top-down illumination, and MP assays were photographed. This imaging technique setup enabled adequate excitation for fluorescence of the induced MP particles, enhancing visibility by producing even lighting, reducing shadows, and highlighting surface details from above. All visible equipment displays were shielded with black cardboard and opaque tape to achieve near-complete darkness. In adherence to strict conditions, the pop-up darkroom remained closed, and only essential personnel in appropriate cotton lab coats were permitted entry to minimize the risk of light and air pollution, mirroring conditions from prior digital photography research [51]. Using optimal conditions (Section 2.5.1), a camera height of 0.6 m above the sample assay yielded a total field of view of 27 cm × 18 cm, with a resolution of 6000 px × 4000 px and a corresponding pixel size of 45 μm × 45 μm. Since all darkroom photography was conducted under constant light conditions, it was kept constant for subsequent analysis once the image classification process was developed.

2.4. Image processing

Our protocol applied a thresholding and segmentation-based approach for image analysis using freeware ImageJ version 1.54j (<https://imagej.net/>). This aimed to assess background noise in dark-frame photographs, analyze particle morphology, optimize the detection of MPs, and obtain image-based counts of induced fluorescent MPs. Manual color thresholding was performed based on Hue, Saturation, and Brightness (HSB) ranges, utilizing pixel intensities of the fluorescent colors specific to the polymers. Following the thresholding procedure, a binary transformation was applied to convert the image into a mask, effectively segregating selected pixels. Edge detection using the 'Find Edges' tool, subsequent thresholding, and the 'Fill Hole' function in ImageJ was used as a closing filter. Additional segmentation was employed using the 'Watershed' tool to separate connected particles. Particle analysis was conducted using the 'Analyze particle' option, and

data regarding particle size (Feret, major, minor axis), particle area, and circularity were recorded. For a precise particle count analysis, we used each polymer size fraction's known mean MP particle areas to identify clustered particles. The number of particles in a cluster was estimated as a ratio of the cluster area to the mean particle surface area. Based on pre-experimental analysis (Section 2.5.1 below), we developed a semi-automated approach for successive image analysis using ImageJ macro and batch processing using the parameters obtained. Compared to fluorescent staining techniques such as Nile Red, which are prone to background fluorescence due to non-specific binding to natural organic matter [46,47], our approach using intrinsically fluorescent MPs eliminates the staining step and significantly reduces background noise. Control samples containing only soil (no MPs) showed no false positive results below the applied threshold, indicating minimal background interference. This contrasts with Nile Red-based studies, which often require organic matter digestion or complex background subtraction to resolve this issue [47,55].

2.5. Experimental design

Experimental analysis was conducted in two phases: a pre-experiment to optimize darkroom parameters and a main experiment testing the developed protocol that used the optimized parameters. Recovery rates were checked for varying conditions and concentrations. A schematic of the experimental design is provided in Fig. 1.

2.5.1. Pre-experiment analysis

To optimize MP detection using UV light photography and image analysis, preliminary tests established optimal imaging conditions and an analytical approach by preparing an image classification workflow. Firstly, fifty manually counted spherical polyethylene (PE) and irregular polylactic acid (PLA) MPs were photographed without soil (MP particles spaced apart on a clean surface to prevent overlap) and with soil (mixed with sieved dry soil to simulate environmental conditions). Three different UV wavelengths and varying camera settings of exposure time, aperture, and ISO were assessed for pure MP particles and MP-soil interference. Optimal fluorescence was achieved at 365 nm UV light, close to the peak excitation of 400 nm for PE and 370 nm for PLA, as given by the manufacturer and literature [52], respectively. The optimal camera settings were 0.2 s exposure, ISO 100, and F5.6. The optimized conditions were used to develop an image classification macro. Image

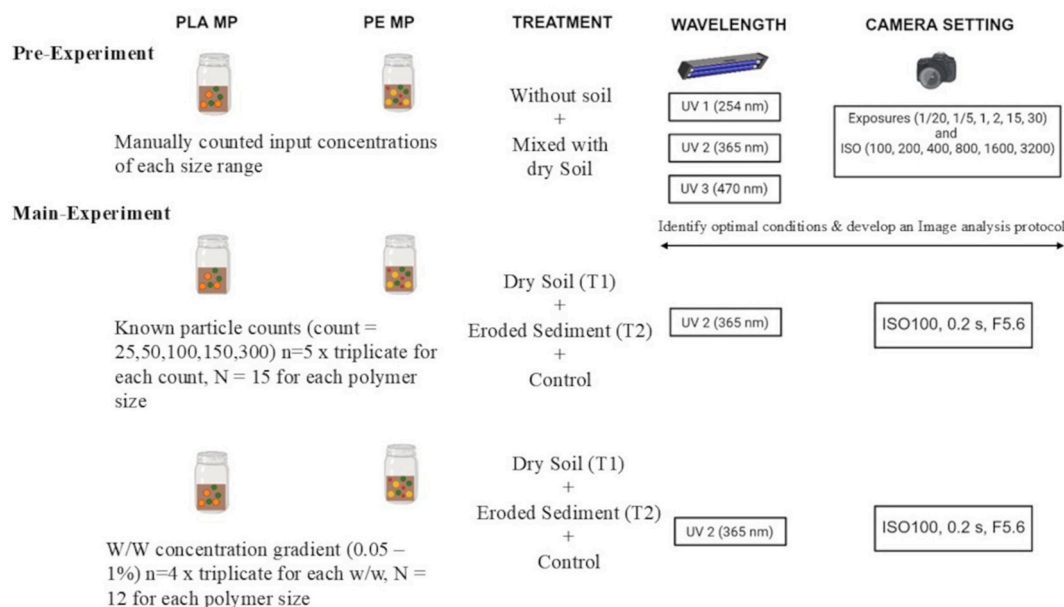


Fig. 1. Schematic showing framework of experimental analysis conducted.

analysis during the pre-experiment was also used to assess particle morphological descriptors (Supplement S1)

To validate the robustness of the image analysis, triplicate samples containing known MP mass (0.001 g, 0.004 g, and 0.007 g) were weighed using a precision balance and manually counted. These samples, without soil, were photographed under optimized UV and camera conditions. The resulting images were processed with the finalized image analysis workflow and compared with manual counts. A strong correlation was observed between the manual and image analysis counts, with Pearson coefficient ($r > 0.9$) for all size ranges. Image counts showed an average absolute deviation of $<8\%$ compared to manual counts, indicating high accuracy (deviation was calculated as the percentage difference between manual and image analysis counts) (Table S1).

Additionally, the relationship between MP weight and particle count was analyzed. PE and PLA MPs across varying size ranges were weighed (0.001–0.1 g) using a fine balance, and triplicates of each weight were photographed under optimized imaging conditions and analyzed using the developed macro. A linear regression model was established, providing a reference curve (particle count vs. weight) for subsequent experiments involving unknown particle counts. This reference curve allowed the estimation of input particle counts for soil samples with MPs added as weight-to-weight (w/w) ratios in subsequent analysis (Fig. 2).

2.5.2. Main Experiment

For the main experiment, we analyzed two treatments: (1) dry soil (Treatment 1) and (2) wet soil mimicking sediment transport due to surface runoff (Treatment 2). For Treatment 1, 10 g of dry soil was mixed with MPs in 750 ml glass jars. For Treatment 2, the soil-MP mixtures (as

in Treatment 1) were combined with 500 ml of distilled water in 750 ml glass jars (Fig. 3A). All prepared samples were kept in a cool and dark environment (refrigerated at $4\text{ }^{\circ}\text{C}$) for one week to enable MP-soil interaction before subsequent analysis. This helped to stabilize the distribution of MPs within the matrices and reduce the potential for surface aggregation or uneven mixing while preserving the polymers' integrity and their fluorescent properties.

To test the protocol's sensitivity and scalability, MPs of varying size ranges (125–150 μm , 250–300 μm , 425–500 μm) were mixed with soil accounting for very low to very high concentration/particle count: (1) Known Particle Counts (25, 50, 100, 150, 300) and (2) w/w Concentration Gradients (0.05 %, 0.1 %, 0.5 %, and 1 % w/w). The reference curve developed in the previous step accurately estimated MP counts for high concentrations. This approach evaluated the protocol's scalability for processing samples with higher microplastic concentrations, where manual particle counting is impractical.

For each treatment and concentrations, MPs were prepared and mixed independently for PE and PLA to avoid visual bias, as fluorescent orange PLA particles (125–150 μm) appeared visually similar to red PE particles (425–500 μm) under UV light. Control treatments without fluorescent PE or PLA were also prepared and analyzed alongside the experimental samples. The laboratory was thoroughly cleaned before and during sample preparation to prevent contamination. Plastic fiber clothing was prohibited, and all analytical tools used were non-plastic except for a white-colored wash bottle.

2.6. MP assay preparation using developed protocol

Standard dry and wet sieving techniques were adapted to recover

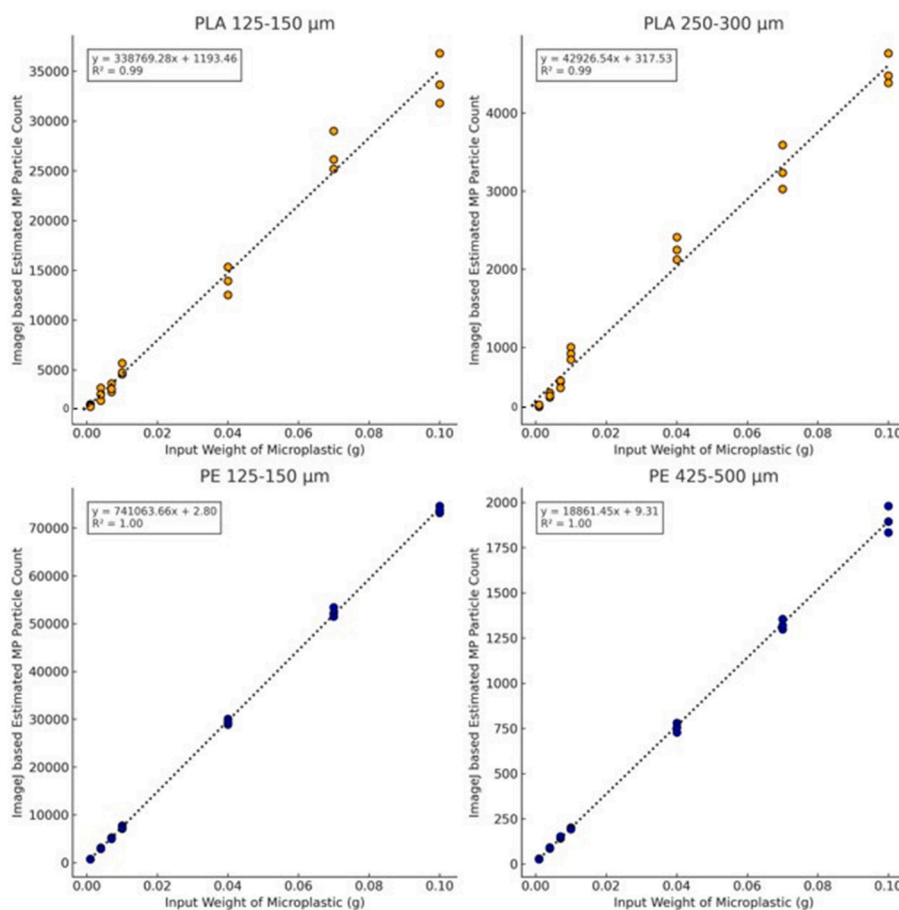


Fig. 2. Reference curve for 125–150 μm PLA, 125–150 μm PE, 250–30 μm PLA, and 425–500 μm PE. Input weight (g) as measured using a fine balance. Estimated particle counts are assessed using image analysis. The dotted black line shows the regression fit.

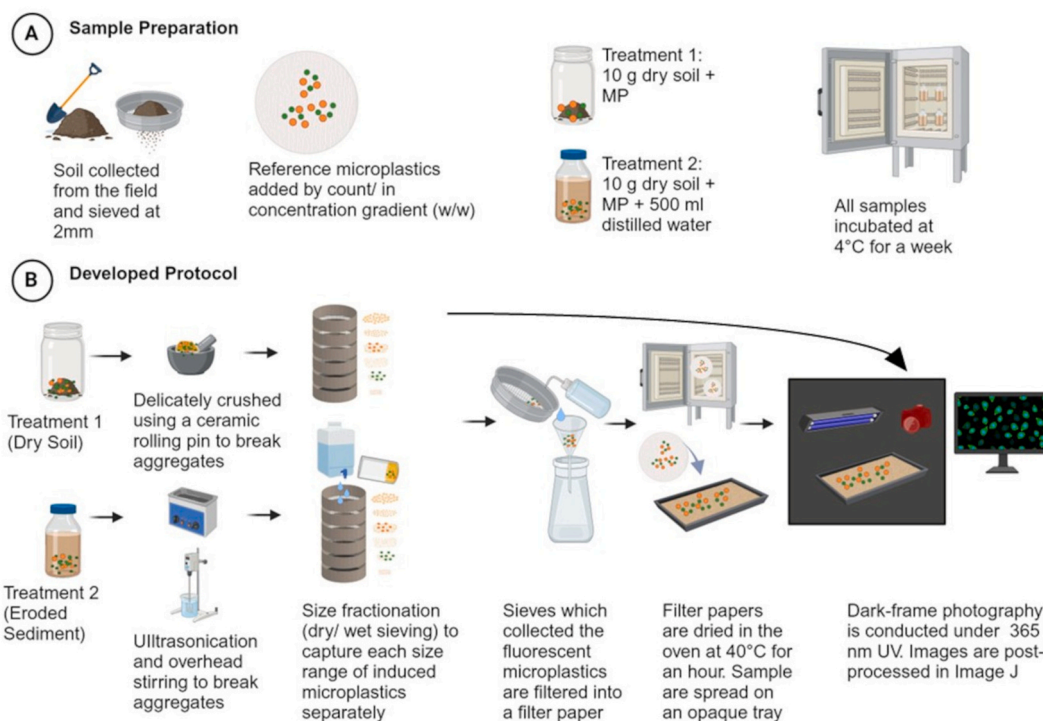


Fig. 3. Steps showing sample preparation processes (A) and preparation of microplastic assays for darkroom photography as per developed protocol (B).

MPs from prepared samples. Samples from Treatment 1 were carefully crushed using a ceramic rolling pin to break agglomerates while minimizing additional fragmentation of induced MPs. The crushed samples were then subjected to dry sieving. For Treatment 2, a dispersing procedure was applied to disaggregate MP-soil clumps. This involved two cycles of magnetic stirring at 500 rpm for 10 min, followed by ultrasonication (130/300 W, 400 kHz) for another 10 min. The dispersed samples were subsequently wet-sieved (Fig. 3B).

For both treatments, a sieve cascade setup with mesh sizes of 1 mm, 500 μm , 400 μm , 300 μm , 250 μm , 150 μm , 100 μm , and 50 μm was employed. This facilitated the separation of MPs and soil particles into designated size fractions, aligning with the size ranges of the induced MPs under investigation (PE: 125–150 μm and 425–500 μm ; PLA: 125–150 μm and 250–300 μm). This method also reduced the initial sample size from 10 g to 2.6 ± 0.3 g to 1.5 ± 0.2 g across all size fractions. During pre-experiment optimization, subsampling protocols were developed based on the experimental setup's best pixel size and field of view. Each gram of sample was subsampled into approximately five portions for smaller size fractions (125–150 μm) and approximately two portions for the largest fraction (425–500 μm). This subsampling strategy ensured uniform distribution of MPs across the sample assay, minimizing clustering, occlusion, and aggregation during UV imaging. The number of subsamples per gram was optimized based on the camera's field of view and detection resolution to ensure accurate particle segmentation while maintaining consistent MP counts across all replicates.

Induced MPs and organic soil particles retained on each sieve were gently washed using a wash bottle and collected on filter paper with a pore size of 0.7 μm . The filters were dried at 40 °C for 1 h. The residual particles were manually spread as a thin layer on 20 cm diameter opaque petri dishes for darkroom photography under UV light. Filters were also photographed to ensure no residual fluorescent MPs remained. To measure the precise MP and soil fraction content, all filters were oven-dried at 100 °C for 1 h and weighed before filtration. Additionally, to check the temporal effect of fluorescence polymers, all sample assays were stored in glass jars with tin lids, and re-analysis was carried out after three months.

2.7. Validation of developed protocol

Recovery was assessed based on particle detection using image processing-based counts and evaluated using key metrics, including precision, recall, and F-score. The validation involved identifying and calculating the true positives (TP, actual MP particles identified), false positives (FP, particles which are not MP but identified as one), and false negatives (FN, MP particles which were unidentified). Further, we calculated for precision (the proportion of true positives that can be trusted) and recall (the proportion of true positives we found). The F-score measures accuracy as the harmonic mean of recall and precision and was used as a balanced measure of detection accuracy. A high F-score indicates that the protocol detects MPs accurately and minimizes errors, making it a robust validation metric.

$$\text{Precision } (P) = \left(\frac{TP}{TP + FP} \right) \quad (1)$$

$$\text{Recall } (R) = \left(\frac{TP}{TP + FN} \right) \quad (2)$$

$$\text{Fscore} = \left(\frac{2 * P * R}{P + R} \right) \quad (3)$$

Recovery was calculated as the ratio of particles detected by image analysis to the estimated/known input particle count:

$$\text{Recovery } (\%) = \frac{\text{Particles Detected by Image Analysis (count)}}{\text{Input Particles (count)}} * 100 \quad (4)$$

To further assess the reliability of the protocol, regression analyses were conducted to evaluate the relationships between input weight added and (1) MP count as detected by image analysis, (2) area as detected from vertical scanning of ImageJ, and (3) volume (cm^3). Volume calculation for PE was done using sphere formulae, given that their shapes were near circular. For irregular PLA, MP particles were assumed to be ellipsoidal, where the major axis corresponded to the largest measured cross-sectional size of the particle and the minor axis corresponded to the smallest measured cross-sectional size. Consequently, in

addition to the major and minor axes, the third dimension of the particles was taken to be equal to the minor axis of the best-fitting ellipse, and particle volume was calculated.

2.8. Statistical analysis

Quantitative data of the obtained microplastic count and precision, recall, F-score, and recovery validation parameters are presented as mean \pm standard deviation (STD). Since the data did not align with a normal distribution, the Mann-Whitney *U* test was used to analyze the difference in recovery across polymer types (PE vs PLA). The Kruskal-Wallis test was used to analyze recovery across the various polymer sizes, and the Wilcoxon Signed-Rank test was used to analyze the difference between the two treatment conditions. Probability levels below 0.05 were considered statistically significant. All statistical analyses and the generation of required vector plots were carried out using Matplotlib v3.6.1 in Python. Scientific illustrations were created using Biorender.

3. Results and discussions

This research introduces a cost-effective, time-efficient protocol using UV-illuminated darkroom photography and image analysis to detect fluorescent MPs (125–500 μm) in soil and sediment samples. The protocol, requiring minimal specialized equipment and standard laboratory tools, enables rapid sample processing—approximately 30 min for Treatment 1 and 90–110 min for Treatment 2. The overall precision across different particle sizes, polymer types, and treatments was $88.7\% \pm 2.9\%$, the recall was $85.2\% \pm 3.1\%$, and the F-score was $86.9\% \pm 2.8\%$, indicating strong reliability and accuracy. Mean precision, recall, and F-scores for each treatment are presented in Table 1, demonstrating consistent performance under Treatment 1 and Treatment 2.

Polymers differ in density, shape, and surface properties, affecting recovery and detection efficiencies [53], and their environmental fate [28]. We checked for two UV-labeled fluorescent polymers: an expensive spherical PE microsphere and an easily accessible, cheaper PLA filament ground into irregular MPs. The recovery rates of PE and PLA MPs were compared across treatments using a Mann-Whitney *U* test, which revealed no statistically significant differences between the two polymers ($U = 5814.5$, $p = 0.436$). This suggests that both fluorescent polymer types can be used effectively. Various studies have focused on several aspects of MP transport within this size range. The effect of vegetation on the horizontal transport of MP [27] used six hundred (MP count) fragments of 0.25–1 mm PE and Polypropylene (PP), analysis of irrigation facilitated vertical transport of low-density PE [22] used 75% 0.5–1 mm spherical PE, study of size and shape of MP on lateral and horizontal migration [28] used 1–3 mm PE and 0.2–3 mm PET spherical particles. To further enhance such microplastic transport studies in agricultural soils in field and lab environments, our results promote the use of commercial and non-commercial fluorescent MP as proxy tracers, which we infer as easily identifiable non-destructively using the developed protocol.

However, the commercially bought spherical PE MPs achieved higher mean recovery rates ($\sim 85\% \pm 5\%$) than the PLA MPs ($\sim 79\% \pm 8\%$) across both treatments (Fig. 4). For samples with smaller input concentrations (MP count = 25, 50, 100), PLA recovery, especially in Treatment 1, was below 70%. This variability highlights potential

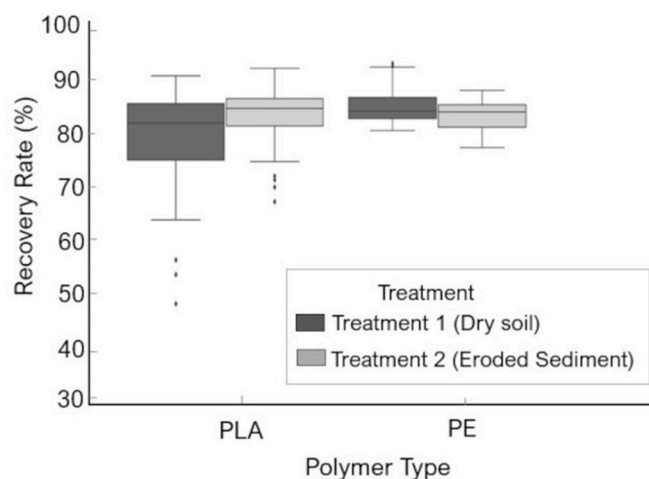


Fig. 4. Recovery rate by polymer type for the two different treatments. The boxes around the median represent the first and third quartiles; whiskers give the minimum and maximum, while the dotted line shows outliers.

challenges in accurately detecting lower concentrations of irregularly shaped PLA particles under dry soil conditions. In contrast, PE MPs consistently recovered above 85% across all input counts and treatments. This could be due to the PE MPs' spherical shape, making them uniform and more straightforward to detect and recover using image analysis, wherein their consistent shape results in fewer particles being misclassified or lost during processing. The fluorophore in the PE microspheres was homogeneously incorporated into the polymer matrix, ensuring consistent fluorescence compared to PLA particles obtained from filaments. Being irregularly shaped, PLA particles may not fluoresce uniformly and, with an MP count of up to 100, may have increased contact with soil particles, leading to adhesion, misidentification, or lower visibility under UV light. The use of grounded PLA from 3D printable filament has been successfully used in MP ecotoxicology studies [54], and given its high recovery rate using our protocol, we suggest using it in MP transport studies to analyze the effect of biodegradable polymers in agricultural soils.

Overall recovery (%) was slightly higher in Treatment 2 than Treatment 1. While Treatment 2 consistently yielded higher mean recoveries across both polymer types and particle sizes, a Wilcoxon Signed-Rank paired test indicated that these differences were marginal and not statistically significant ($W = 100.0$, $p = 0.055$). This could be due to the particle separation efficiency where wet conditions help suspend MPs, making them easier to sieve and separate. Wet sieving makes MPs more likely to be separated from soil aggregates or organic matter adhering to MPs due to the dispersing effect of water. Additionally, the ultrasonication and magnetic stirring used in Treatment 2 minimizes the chances of MPs being retained in soil aggregates compared to dry sieving in Treatment 1, which could be an important aspect if fluorescent MPs are used in long-term experiments. Also, while sample preparation, the allowance of sedimentation for Treatment 2 ensures that particles settle individually, avoiding stacks or aggregates that can complicate detection. Additionally, drying the sample before sample assay preparation for darkroom photography ensures that

Table 1

The precision, recall, and F-score values for the reference polymers in different treatments.

| Polymer Type | Size (μm) | Precision (mean \pm STD) | | Recall (mean \pm STD) | | F-Score (mean \pm STD) | |
|--------------|------------------------|----------------------------|-----------------|-------------------------|-----------------|--------------------------|-----------------|
| | | Treatment 1 | Treatment 2 | Treatment 1 | Treatment 2 | Treatment 1 | Treatment 2 |
| PLA | 125–150 | 0.96 \pm 0.09 | 0.98 \pm 0.05 | 0.72 \pm 0.16 | 0.80 \pm 0.09 | 0.82 \pm 0.14 | 0.87 \pm 0.07 |
| | 250–300 | 0.97 \pm 0.04 | 0.95 \pm 0.08 | 0.82 \pm 0.08 | 0.85 \pm 0.05 | 0.89 \pm 0.06 | 0.90 \pm 0.05 |
| PE | 125–150 | 0.98 \pm 0.04 | 0.97 \pm 0.06 | 0.84 \pm 0.03 | 0.83 \pm 0.04 | 0.90 \pm 0.02 | 0.89 \pm 0.04 |
| | 425–500 | 0.96 \pm 0.06 | 0.97 \pm 0.03 | 0.88 \pm 0.05 | 0.88 \pm 0.05 | 0.91 \pm 0.04 | 0.92 \pm 0.03 |

particles are better separated and do not form clusters or adhere to each other. Regardless, there is no statistical significance between the two treatments, with a wet soil treatment (valuable for soils and sediments) offering a marginal improvement in separation efficiency.

Particle size significantly influenced recovery rates, as smaller particles (125–150 μm) generally exhibited lower recovery compared to larger particles (250–300 μm and 425–500 μm) (Fig. 5). A Kruskal-Wallis test revealed significant differences in recovery rates across the three size categories (125–150 μm , 250–300 μm , and 425–500 μm). Pairwise Mann-Whitney U tests confirmed the significant differences were amongst 125–150 μm vs. 250–300 μm ($U = 2109.0$, $p < 0.01$), 125–150 μm vs. 425–500 μm ($U = 1289$, $p < 0.001$), and 250–300 μm vs. 425–500 μm : ($U = 1015$, $p < 0.01$), indicating that recovery rates increase significantly with particle size. This pattern was consistent across both treatments, highlighting the challenges of detecting smaller particles. For PE MPs in Treatment 1, recovery rates for smaller particles averaged $85\% \pm 8\%$, while larger particles achieved recoveries close to $95\% \pm 3\%$. Similarly, PLA MPs showed lower recovery rates for the smallest size fraction ($75\% \pm 12\%$) compared to larger sizes ($85\% \pm 5\%$). Smaller particles (125–150 μm) have a reduced surface area, producing less fluorescence under UV light. This makes it harder to identify and differentiate from soil particles. Additionally, loamy soil was used, with 52.1% silt and clay content, which has a high specific surface area and can adhere firmly to smaller MPs due to electrostatic forces and van der Waals interactions. The use of a UV light box and camera setup to identify Nile red fluoresced microplastics from soil has been previously shown by Ref. [54], although they could successfully classify 0.63–1.0 mm and >1.0–5.0 mm for particles and fragments after organic matter removal and density separation. Comparatively, our recovery rates are appropriate for MP transport studies.

The sensitivity of the protocol was assessed by evaluating recovery rates across input concentrations, ranging from 25 to 300 particles (manually counted) to well over 20,000 particles (input as w/w), confirming the protocol's reliability across a wide range of concentrations. PLA MPs exhibited slightly lower recovery rates at lower input counts than PE MPs; however, this discrepancy diminished at higher concentrations, with recovery stabilizing beyond 100 particles. The rate of change in recovery was highest between 25 and 50 particles (+4.67%) and significantly diminished for larger input counts, indicating method sensitivity to smaller particle concentrations. Negative rates of change were observed sporadically at very high input counts, reflecting potential fluctuations in recovery efficiency (Fig. 6). Additionally, the linear regression analysis between MP Weight Added (g) and particle volume, area, and MP observed counts demonstrated strong linear relationships across all particle sizes, polymer types, and treatments ($R^2 > 0.98$ in all cases) (Table S2), furthering the protocol's reliability.

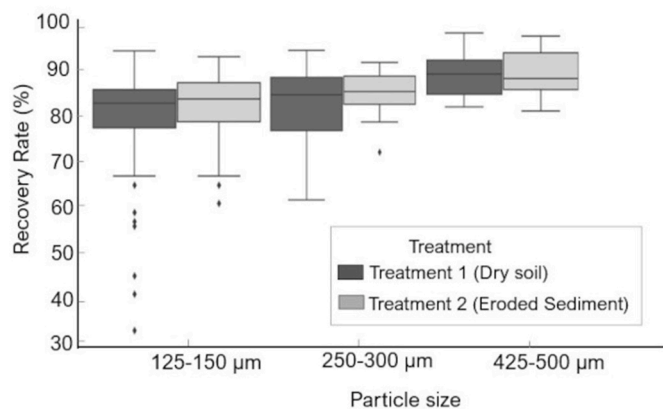


Fig. 5. Recovery rate by microplastic size for the two different treatments. The boxes around the median represent the first and third quartiles; whiskers give the minimum and maximum, while the dotted line shows outliers.

By eliminating the need for complex separation or digestion steps, this protocol offers an efficient and accessible alternative for MP transport research in soil and sediment systems. Unlike Nile Red staining, which can encounter challenges such as discoloration of colored polymers, interference from natural organic matter, and background fluorescence from filter paper, leading to potential overestimations of microplastic particle count [46]. In contrast, our protocol using pre-labeled fluorescent MPs avoids these issues entirely. The negligible false positive rate observed in our control tests confirms the low background signal, and our high precision values (up to 98%, Table 1) reflect the method's robustness in distinguishing MPs from the soil matrix. This highlights a key advantage over Nile Red-based techniques, which often require additional preprocessing steps to mitigate background interference [47,55]. Therefore, our method simplifies detection and improves reliability, particularly beneficial for microplastic transport studies. A systematic re-analysis of all MP particles stored in sieved samples for three months exhibited minimal recovery loss ($\sim 4.8 \pm 1.9\%$), attributed primarily to handling. All particles retained fluorescence intensity above detectable levels regardless of polymer type or size. While our results confirm the short-term fluorescence stability over a 3-month storage period, we believe longer-term assessments are essential, particularly for studies involving extended field campaigns or multi-seasonal monitoring. Future research could explore fluorescence stability over longer temporal scales or under variable environmental conditions (e.g., UV exposure, humidity, or temperature fluctuations) to ensure continued marker viability.

Also, darkroom photography for Nile Red fluoresced MPs has been increasingly adopted [55]. This study highlights a cost-effective pop-up darkroom tent as a viable alternative. The pop-up tent's compact design minimizes laboratory contamination risks, a critical concern in MP research. Any contamination can be minimized by setting image analysis thresholding and segmenting parameters based on pre-characterized MP morphology.

While this protocol offers several advantages in terms of cost efficiency, speed, and simplicity, it exhibits lower recovery rates for smaller MPs (particularly those in the 125–150 μm range). This limitation is consistent with the results of previous studies [56,57] and can be attributed to two primary factors: (1) the limited resolution and sensitivity of darkroom photography in detecting weak fluorescence signals from finer particles, and (2) the accumulation of residual organic matter and soil particulates during sample preparation, which can obscure or scatter fluorescence. Despite these pre-treatment steps, residual organic debris may still scatter light or create fluorescence artifacts that reduce contrast or mimic the appearance of MPs. Although thresholding and morphology-based segmentation reduce this effect, it cannot be fully eliminated, particularly in fine fractions or more organic-rich samples. These factors contribute to a size-dependent recovery trend, particularly affecting the smallest MPs in the tested range. Further studies could incorporate higher-resolution imaging equipment and advanced image analysis techniques, such as machine learning-based particle detection, edge-enhancement algorithms, or fluorescence thresholding with background subtraction to improve detection accuracy for smaller MPs, especially in heterogeneous sediment samples.

This protocol was developed for controlled MP transport studies in which known quantities of pre-labeled PE or PLA particles are added as tracers in laboratory or field experiments. Its simplicity, cost-effectiveness, and non-destructive nature are well-suited for high-throughput sample processing and long-term monitoring without complex extraction procedures. Potential applications include tracking MP movement in erosion plots, simulating vertical transport in infiltration columns, and studying temporal redistribution across cropping cycles. Furthermore, the statistically significant results demonstrate the practical relevance for controlled research designs where accurate and repeatable detection is essential. While the current study was conducted under laboratory conditions, the protocol is intended for use in designed field experiments with known MP inputs. Factors such as soil variability

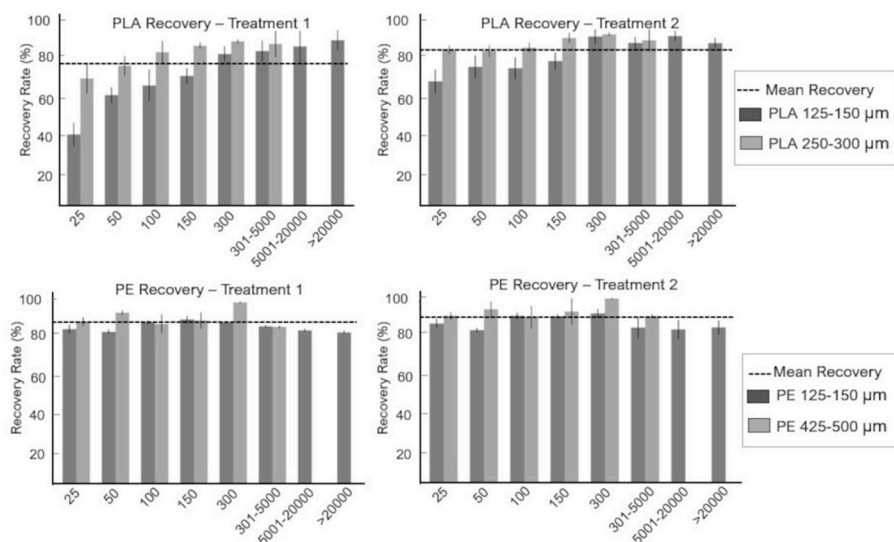


Fig. 6. Recovery rate by microplastic particle concentration (count) for the two different treatments. The bars represent recovery rates, while the error bar indicates standard deviation. The dotted line represents the mean recovery rate.

and MP burial depth may cause detection issues in such environments, but the method remains applicable with minimal adjustments. Future studies could investigate calibration steps for different field conditions to enhance reliability. Furthermore, the method works well within these controlled contexts, but limitations remain in detecting smaller particles and applying the protocol in highly organic or heterogeneous soils. Future adaptations—such as improved optics, image resolution, or semi-automatic segmentation—could help overcome these challenges if higher sensitivity is required while preserving the protocol's overall accessibility.

4. Conclusion

This study presents a cost-effective and reliable protocol for detecting microplastic transport on the soil surface or within the soil column while using fluorescent microplastics (MPs) added in experimental setups. The protocol demonstrated high accuracy across particle sizes, polymer types, and treatments, with mean precision, recall, and F-scores exceeding 85 %. While PE MPs consistently showed higher recovery rates due to their spherical shape and uniform fluorescence, PLA MPs also performed effectively, making both polymers suitable as tracers in MP transport studies. During sample preparation, recovery rates improved under wet sediment conditions due to enhanced particle separation. Overall, this protocol provides a robust, scalable framework for advancing MP research in agricultural soils, offering a practical tool for understanding MP fate and transport across diverse environmental conditions.

Funding

This research received funding from the European Union's Horizon 2020 research and innovation program under the Marie Skłodowska-Curie Grant Agreement No. 955334, project "Macro and Microplastic in Agricultural Soil Systems" – SOPLAS.

CRediT authorship contribution statement

Saunak Sinha Ray: Writing – review & editing, Writing – original draft, Visualization, Validation, Software, Methodology, Formal analysis, Data curation, Conceptualization. **David Zumr:** Writing – review & editing, Methodology, Formal analysis. **Florian Wilken:** Writing – review & editing, Methodology, Conceptualization. **Tomáš Dostál:**

Writing – review & editing, Supervision, Resources, Project administration, Methodology, Funding acquisition. **Peter Fiener:** Writing – review & editing, Supervision, Resources, Project administration, Methodology, Funding acquisition, Conceptualization.

Declaration of competing interest

The authors declare that they have no known competing financial interests or personal relationships that could have appeared to influence the work reported in this paper.

Acknowledgments

We want to thank Raphael Rehm and Martin Neumann for their help in the laboratory experimental setup, Adam Tejkl for his help with modifying the darkroom table setup, and Raquel Nogueira Rizzotto Falcao for her help as an operator in the darkroom photography.

Appendix A. Supplementary data

Supplementary data to this article can be found online at <https://doi.org/10.1016/j.polymeresting.2025.108824>.

Data availability

Data will be made available on request.

References

- [1] M.O. Rodrigues, N. Abrantes, F.J.M. Gonçalves, H. Nogueira, J.C. Marques, A.M. M. Gonçalves, Spatial and temporal distribution of microplastics in water and sediments of a freshwater system (Antuã River, Portugal), *Sci. Total Environ.* 633 (Aug. 2018) 1549–1559, <https://doi.org/10.1016/J.SCITOTENV.2018.03.233>.
- [2] L. Van Cauwenbergh, L. Devriese, F. Galgani, J. Robbins, C.R. Janssen, Microplastics in sediments: a review of techniques, occurrence and effects, *Mar. Environ. Res.* 111 (Oct. 2015) 5–17, <https://doi.org/10.1016/J.MARENRES.2015.06.007>.
- [3] L. Yang, Y. Zhang, S. Kang, Z. Wang, C. Wu, Microplastics in soil: a review on methods, occurrence, sources, and potential risk, *Sci. Total Environ.* 780 (Aug. 2021) 146546, <https://doi.org/10.1016/J.SCITOTENV.2021.146546>.
- [4] S. Sridharan, M. Kumar, L. Singh, N.S. Bolan, M. Saha, Microplastics as an emerging source of particulate air pollution: a critical review, *J. Hazard Mater.* 418 (Sep. 2021) 126245, <https://doi.org/10.1016/J.JHAZMAT.2021.126245>.
- [5] A.A. Horton, A. Walton, D.J. Spurgeon, E. Lahive, C. Svendsen, Microplastics in freshwater and terrestrial environments: evaluating the current understanding to identify the knowledge gaps and future research priorities, *Sci. Total Environ.* 586 (May 2017) 127–141, <https://doi.org/10.1016/J.SCITOTENV.2017.01.190>.

- [6] W. Li, et al., Microplastics in agricultural soils: extraction and characterization after different periods of polythene film mulching in an arid region, *Sci. Total Environ.* 749 (Dec. 2020) 141420, <https://doi.org/10.1016/J.SCITOTENV.2020.141420>.
- [7] R.W. Chia, J.Y. Lee, M. Lee, S. Lee, Comparison of microplastic characteristics in mulched and greenhouse soils of a major agriculture area, Korea, *J. Polym. Environ.* 31 (5) (May 2023) 2216–2229, <https://doi.org/10.1007/S10924-022-02746-1/FIGURES/11>.
- [8] D. Briassoulis, Agricultural plastics as a potential threat to food security, health, and environment through soil pollution by microplastics: problem definition, *Sci. Total Environ.* 892 (Sep. 2023) 164533, <https://doi.org/10.1016/J.SCITOTENV.2023.164533>.
- [9] E.H. Lwanga, et al., Review of microplastic sources, transport pathways and correlations with other soil stressors: a journey from agricultural sites into the environment, *Chem. Biol. Technol. Agric.* 9 (1) (Feb. 2022) 1–20, <https://doi.org/10.1186/S40538-021-00278-9>, 2022 9:1.
- [10] V.C. Shruti, G. Kutralam-Muniasamy, Bioplastics: missing link in the era of microplastics, *Sci. Total Environ.* 697 (Dec. 2019) 134139, <https://doi.org/10.1016/J.SCITOTENV.2019.134139>.
- [11] M. Vithanage, S. Ramanayaka, S. Hasinithara, A. Navaratne, Compost as a carrier for microplastics and plastic-bound toxic metals into agroecosystems, *Curr Opin Environ Sci Health* 24 (Dec. 2021) 100297, <https://doi.org/10.1016/J.COESH.2021.100297>.
- [12] M.D. Hatinoğlu, F.D. Sanin, Sewage sludge as a source of microplastics in the environment: a review of occurrence and fate during sludge treatment, *J. Environ. Manag.* 295 (Oct. 2021) 113028, <https://doi.org/10.1016/J.JENVMAN.2021.113028>.
- [13] S. Guo, et al., Organic fertilizer and irrigation water are the primary sources of microplastics in the facility soil, Beijing, *Sci. Total Environ.* 895 (Oct. 2023) 165005, <https://doi.org/10.1016/J.SCITOTENV.2023.165005>.
- [14] M. Rezaei, S. Abbasi, H. Pourmahmood, P. Oleszczuk, C. Ritsema, A. Turner, Microplastics in agricultural soils from a semi-arid region and their transport by wind erosion, *Environ. Res.* 212 (Sep. 2022) 113213, <https://doi.org/10.1016/J.ENVRES.2022.113213>.
- [15] A.A. Horton, S.J. Dixon, Microplastics: an introduction to environmental transport processes, *Wiley Interdiscipl. Rev.: Water* 5 (2) (Mar. 2018) e1268, <https://doi.org/10.1002/WAT2.1268>.
- [16] B. Baensch-Baltruschat, B. Kocher, C. Kochleus, F. Stock, G. Reifferscheid, Tyre and road wear particles - a calculation of generation, transport and release to water and soil with special regard to German roads, *Sci. Total Environ.* 752 (Jan. 2021) 141939, <https://doi.org/10.1016/J.SCITOTENV.2020.141939>.
- [17] S. Zhang, X. Liu, X. Hao, J. Wang, Y. Zhang, Distribution of low-density microplastics in the mollisol farmlands of northeast China, *Sci. Total Environ.* 708 (Mar. 2020) 135091, <https://doi.org/10.1016/J.SCITOTENV.2019.135091>.
- [18] M. Kumar, et al., Microplastics as pollutants in agricultural soils, *Environ. Pollut.* 265 (Oct. 2020) 114980, <https://doi.org/10.1016/J.ENVPOL.2020.114980>.
- [19] B. van Schothorst, N. Beriot, E. Huerta Lwanga, V. Geissen, Sources of light density microplastic related to two agricultural practices: the use of compost and plastic mulch, *Environments - MDPI* 8 (4) (Apr. 2021) 36, <https://doi.org/10.3390/ENVIRONMENTS8040036/S1>.
- [20] P. van den Berg, E. Huerta-Lwanga, F. Corradini, V. Geissen, Sewage sludge application as a vehicle for microplastics in eastern Spanish agricultural soils, *Environ. Pollut.* 261 (Jun. 2020) 114198, <https://doi.org/10.1016/J.ENVPOL.2020.114198>.
- [21] L. Nizzetto, G. Bussi, M.N. Futter, D. Butterfield, P.G. Whitehead, A theoretical assessment of microplastic transport in river catchments and their retention by soils and river sediments, *Environ Sci Process Impacts* 18 (8) (Aug. 2016) 1050–1059, <https://doi.org/10.1039/C6EM00206D>.
- [22] Z. Zhao, et al., Irrigation-facilitated low-density polyethylene microplastic vertical transport along soil profile: an empirical model developed by column experiment, *Ecotoxicol. Environ. Saf.* 247 (Dec. 2022) 114232, <https://doi.org/10.1016/J.ECOENV.2022.114232>.
- [23] W. Li, G. Brunetti, C. Zafiu, M. Kunaschk, M. Debreczeby, C. Stumpp, Experimental and simulated microplastics transport in saturated natural sediments: impact of grain size and particle size, *J. Hazard Mater.* 468 (Apr. 2024) 133772, <https://doi.org/10.1016/J.JHAZMAT.2024.133772>.
- [24] J. Li, Y. Song, Y. Cai, Focus topics on microplastics in soil: analytical methods, occurrence, transport, and ecological risks, *Environ. Pollut.* 257 (Feb. 2020) 113570, <https://doi.org/10.1016/J.ENVPOL.2019.113570>.
- [25] J. Xu, et al., Nano- and micro-plastic transport in soil and groundwater environments: sources, behaviors, theories, and models, *Sci. Total Environ.* 904 (Dec. 2023) 166641, <https://doi.org/10.1016/J.SCITOTENV.2023.166641>.
- [26] R. Rehm, T. Zeyer, A. Schmidt, P. Fiener, Soil erosion as transport pathway of microplastic from agriculture soils to aquatic ecosystems, *Sci. Total Environ.* 795 (Nov. 2021) 148774, <https://doi.org/10.1016/J.SCITOTENV.2021.148774>.
- [27] N. Han, Q. Zhao, H. Ao, H. Hu, C. Wu, Horizontal transport of macro- and microplastics on soil surface by rainfall induced surface runoff as affected by vegetations, *Sci. Total Environ.* 831 (Jul. 2022) 154989, <https://doi.org/10.1016/J.SCITOTENV.2022.154989>.
- [28] X. Zhang, et al., Size/shape-dependent migration of microplastics in agricultural soil under simulative and natural rainfall, *Sci. Total Environ.* 815 (Apr. 2022) 152507, <https://doi.org/10.1016/J.SCITOTENV.2021.152507>.
- [29] R. Rehm, P. Fiener, Model-based analysis of erosion-induced microplastic delivery from arable land to the stream network of a mesoscale catchment, *SOIL* 10 (1) (Mar. 2024) 211–230, <https://doi.org/10.5194/SOIL-10-211-2024>.
- [30] S. Park, I. Kim, W.H. Jeon, H.S. Moon, Exploring the vertical transport of microplastics in subsurface environments: lab-scale experiments and field evidence, *Hydrol. J. Contam. Hydrol.* 257 (Jul. 2023) 104215, <https://doi.org/10.1016/J.JCONHYD.2023.104215>.
- [31] J. Gao, et al., Vertical migration of microplastics in porous media: multiple controlling factors under wet-dry cycling, *J. Hazard Mater.* 419 (Oct. 2021) 126413, <https://doi.org/10.1016/J.JHAZMAT.2021.126413>.
- [32] N.A. Forster, S.C. Wilson, M.K. Tighe, Examining sampling protocols for microplastics on recreational trails, *Sci. Total Environ.* 818 (Apr. 2022) 151813, <https://doi.org/10.1016/J.SCITOTENV.2021.151813>.
- [33] S. Zhang, X. Yang, H. Gertsen, P. Peters, T. Salánki, V. Geissen, A simple method for the extraction and identification of light density microplastics from soil, *Sci. Total Environ.* 616–617 (Mar. 2018) 1056–1065, <https://doi.org/10.1016/J.SCITOTENV.2017.10.213>.
- [34] D. Thomas, B. Schütze, W.M. Heinze, Z. Steinmetz, Sample preparation techniques for the analysis of microplastics in soil—a review, *Sustainability* 12 (21) (Oct. 2020) 9074, <https://doi.org/10.3390/SU12219074>, 2020, Vol. 12, Page 9074.
- [35] Y. Huang, Q. Liu, W. Jia, C. Yan, J. Wang, Agricultural plastic mulching as a source of microplastics in the terrestrial environment, *Environ. Pollut.* 260 (May 2020) 114096, <https://doi.org/10.1016/J.ENVPOL.2020.114096>.
- [36] T. Maes, R. Jessop, N. Wellner, K. Haupt, A.G. Mayes, A rapid-screening approach to detect and quantify microplastics based on fluorescent tagging with Nile Red, *Sci. Rep.* (1) (Mar. 2017) 1–10, <https://doi.org/10.1038/srep44501>, 2017 7:1, vol. 7.
- [37] K.S. Black, S. Athey, P. Wilson, D. Evans, The use of particle tracking in sediment transport studies: a review, *Geol. Soc. Spec. Publ.* 274 (2007) 73–91, <https://doi.org/10.1144/GSL.SP.2007.274.01.09>.
- [38] R.A. Hardy, J.N. Quinton, M.R. James, P. Fiener, J.M. Pates, High precision tracing of soil and sediment movement using fluorescent tracers at hillslope scale, *Earth Surf. Process. Landf.* 44 (5) (Apr. 2019) 1091–1099, <https://doi.org/10.1002/ESP.4557>.
- [39] H. Laermans, M. Lehmann, M. Klee, M.G.J. Löder, S. Gekle, C. Bogner, Tracing the horizontal transport of microplastics on rough surfaces, *Microplastics and Nanoplastics* 1 (1) (Jul. 2021) 1–12, <https://doi.org/10.1186/S43591-021-00010-2>, 2021 1:1.
- [40] V.S. Mukhanov, D.A. Litvinyuk, E.G. Sakhon, A.V. Bagaev, S. Veerasingam, R. Venkatchalapathy, A new method for analyzing microplastic particle size distribution in marine environmental samples, *Ecol. Montenegrina* 23 (Oct. 2019) 77–86, <https://doi.org/10.37828/EM.2019.23.10>.
- [41] J. Lorenzo-Navarro, et al., SMAAC: a system for microplastics automatic counting and classification, *IEEE Access* 8 (2020) 25249–25261, <https://doi.org/10.1109/ACCESS.2020.2970498>.
- [42] V. Wegmayr, A. Sahin, B. Saemundsson, J.M. Buhmann, Instance Segmentation for the Quantification of Microplastic Fiber Images, 2020.
- [43] M.G.J. Löder, G. Gerdt, Methodology used for the detection and identification of microplastics—a critical appraisal, *Marine Anthropogenic Litter* (Jan. 2015) 201–227, https://doi.org/10.1007/978-3-319-16510-3_8/FIGURES/7.
- [44] C. Zarfl, Promising techniques and open challenges for microplastic identification and quantification in environmental matrices, *Anal. Bioanal. Chem.* 411 (17) (Jul. 2019) 3743–3756, <https://doi.org/10.1007/S00126-019-01763-9/FIGURES/2>.
- [45] S. Pimpke, P.A. Dias, G. Gerdt, Automated identification and quantification of microfibres and microplastics, *Anal. Methods* 11 (16) (Apr. 2019) 2138–2147, <https://doi.org/10.1039/C9AY00126C>.
- [46] V.C. Shruti, F. Pérez-Guevara, P.D. Roy, G. Kutralam-Muniasamy, Analyzing microplastics with Nile Red: emerging trends, challenges, and prospects, *J. Hazard Mater.* 423 (Feb. 2022) 127171, <https://doi.org/10.1016/J.JHAZMAT.2021.127171>.
- [47] J.C. Prata, J.R. Alves, J.P. Da Costa, A.C. Duarte, T. Rocha-Santos, Major Factors Influencing the Quantification of Nile Red Stained Microplastics and Improved Automatic Quantification (MP-VAT 2.0), 2020, <https://doi.org/10.1016/j.scitotenv.2020.137498>.
- [48] N.A. Forster, S.C. Wilson, M.K. Tighe, Microplastic surface retention and mobility on hiking trails, *Environ. Sci. Pollut. Control Ser.* 30 (16) (Apr. 2023) 46368–46382, <https://doi.org/10.1007/S11356-023-25635-Z/TABLES/6>.
- [49] L. Vaught, E. Gonzalez, J.L. Meyer, A.A. Polycarpou, Rapid qualification of fused filament fabrication thermoplastics for cryogenic applications, *Polym. Test.* 129 (Dec. 2023) 108288, <https://doi.org/10.1016/J.POLYMERTESTING.2023.108288>.
- [50] D. Zumr, Agricultural land degradation in the Czech republic, *Handb. Environ. Chem.* 121 (2023) 35–58, <https://doi.org/10.1007/978-92-928-928/TABLES/1>.
- [51] J. Dudas, L.M. Wu, C. Jung, G.H. Chapman, Z. Koren, I. Koren, Identification of infield defect development in digital image sensors 6502 (Feb. 2007) 319–330, <https://doi.org/10.1117/12.704563>.
- [52] F. Yang, et al., Novel AIE luminescent tetraphenylethene-doped poly (lactic acid) composites for fused deposition modeling and their application in fluorescent analysis of 3D printed products, *Compos. B Eng.* 219 (Aug. 2021) 108898, <https://doi.org/10.1016/J.COMPOSITESB.2021.108898>.
- [53] Y. Huang, et al., Quantifying the influence of size, shape, and density of microplastics on their transport modes: a modeling approach, *Mar. Pollut. Bull.* 203 (Jun. 2024) 116461, <https://doi.org/10.1016/J.MARPOLBUL.2024.116461>.
- [54] E. Hengstmann, E.K. Fischer, Nile red staining in microplastic analysis—proposal for a reliable and fast identification approach for large microplastics, *Environ. Monit. Assess.* 191 (10) (Oct. 2019) 1–9, <https://doi.org/10.1007/S10661-019-7786-4/FIGURES/3>.
- [55] J.C. Prata, V. Reis, J.T.V. Matos, J.P. da Costa, A.C. Duarte, T. Rocha-Santos, A new approach for routine quantification of microplastics using Nile Red and automated

- software (MP-VAT), *Sci. Total Environ.* 690 (Nov. 2019) 1277–1283, <https://doi.org/10.1016/J.SCITOTENV.2019.07.060>.
- [56] G. Erni-Cassola, M.I. Gibson, R.C. Thompson, J.A. Christie-Oleza, Lost, but found with Nile red: a novel method for detecting and quantifying small microplastics (1 mm to 20 μm) in environmental samples, *Environ. Sci. Technol.* 51 (23) (Dec. 2017) 13641–13648, https://doi.org/10.1021/ACS.EST.7B04512/SUPPL_FILE/ES7B04512_SI_001. PDF.
- [57] M. Giardino, V. Balestra, D. Janner, R. Bellopede, Automated method for routine microplastic detection and quantification, *Sci. Total Environ.* 859 (Feb. 2023) 160036, <https://doi.org/10.1016/J.SCITOTENV.2022.160036>.